Signature of Ballistic Band-tails Tunneling Current in Tunnel FET

Jasper Bizindavyi, Anne S. Verhulst, Bart Sorée, *Member, IEEE*, and Guido Groeseneken, *Fellow, IEEE*

***Abstract*— To improve the interpretation of tunnel field-effect transistor (TFET) measurements, we theoretically identify the signatures of ballistic band-tails tunneling (BTT) current in the transfer and output characteristics of TFETs. In particular, we demonstrate that the temperature dependence of a BTT-dominated subthreshold swing (SS) is in agreement with reported experimental results. We explain how the temperature dependence of the output characteristics can be used to distinguish between a current dominated by BTT or a current dominated by trap-assisted tunneling. Lastly, we propose an expression that relates the energetic extension of the quasi-extended band-tails states in the bandgap to the onset voltage for tunneling.**

***Index Terms*— Tunnel field-effect transistor (TFET), band-tails, subthreshold swing (SS), III-V semiconductor, trap-assisted tunneling (TAT).**

I. Introduction

TUNNEL field-effect transistors (TFET) are steep-slope devices for which the subthreshold swing (SS) can reach values that go below the lower-limit of the thermally-restricted SS ($60\,\mathrm{mV/dec}$ at room temperature) of the metal-oxide-semiconductor FET (MOSFET) [1]–[3]. This sub-thermionic SS, achieved through quantum-mechanical (QM) band-to-band tunneling (BTBT), makes the TFET a promising device for future ultra-low power logic applications [3], [4].

Currently, the main challenge for TFETs consists of successfully combining a sub-thermionic SS with a sufficiently high drive-current at low operating voltages [5]. To explore the potential causes for sub-optimal SS performance of TFET devices, models are being developed for phonon-assisted tunneling (PAT) [6], trap-assisted tunneling (TAT) [7], [8], Auger generated leakage currents [9] and high-doping-induced band-tails tunneling (BTT) [10]–[16]. So far, investigations of the performance impact of high-doping-induced band-tails in TFETs have mostly been either purely predictive [10]–[12] or qualitative [13] in their approach. Two recent studies link experiment and model: in Ref. [14] a simple model is proposed to extract the band edge decay parameter from experimental TFET data, while in Ref. [15], the impact of random dopant-induced band-tails states on the SS variability has been investigated. However, there remains a need for a more rigorous model and clearer understanding of the various ways in which high-doping-induced band-tails manifest themselves in TFETs, which will facilitate the interpretation of measurement results.

In this work, we use our calibrated (based on Esaki diodes) semi-classical (SC) model for ballistic BTT [16] to identify the signatures of a high-doping-induced BTT current in the transfer and output characteristics. In particular, we focus on the BTT-induced temperature dependence of the TFET performance. In addition, we compare the signatures of a BTT-dominated current with those of a TAT-dominated current.

Manuscript received Month Day, 2020; accepted Month Day, 2020. Date of publication Month Day, 2020; date of current version Month Day, 2020. J. Bizindavyi gratefully acknowledges FWO-Vlaanderen for a Strategic Basic Research PhD fellowship. This work was supported by imec's Industrial Affiliation Program. The review of this letter was arranged by Editor X. X. (Corresponding author: Jasper Bizindavyi.)

J. Bizindavyi and G. Groeseneken are with imec, Leuven 3001, Belgium, and also with the Department of Electrical Engineering, Katholieke Universiteit Leuven, Leuven 3001, Belgium.

A. S. Verhulst is with imec, Leuven 3001, Belgium.

B. Sorée is with imec, Leuven 3001, Belgium, and with the Department of Electrical Engineering, Katholieke Universiteit Leuven, Leuven 3001, Belgium, and also with the Department of Physics, Universiteit Antwerpen, Antwerp 2020, Belgium.

II. Simulation models and device structure

The device under investigation is a pocketed *p-n-i-n* homostructure $In_{0.53}Ga_{0.47}As$ TFET and its schematic structure is shown in Fig. 1. The conventional BTBT current, I_{BTBT}, is determined using a calibrated dynamic non-local SC model [16], [17]. The high-doping-induced BTT contributions, I_{BTT}, are calculated using our calibrated SC ballistic BTT model, which assumes that the band-tails states originate from high-doping-induced structural disorder (other sources of structural or thermal disorder are not considered) [16], [18]. In particular, an artificial dispersion relation (Eq. (1) in Ref. [16]) is assumed to describe the band-tails states such that the following exponential energy dependence for the band-tails density-of-states (DOS) is obtained, which is in agreement with both theoretical assessments and experimental measurements (Fig. 2):

$$g_{\mathrm{bts,c/v}}(E_{\mathrm{bts}}) = \frac{k_{1,\mathrm{c/v}}^3}{3\pi^2 E_{0,\mathrm{c/v}}} \exp\left(\pm\frac{E_{\mathrm{bts}} - E_{1,\mathrm{c/v}}}{E_{0,\mathrm{c/v}}}\right) \quad (1)$$

where $+(-)$ refers to the conduction(valence) band-tails, $E_{1,\mathrm{c/v}}$ and $k_{1,\mathrm{c/v}}$ determine the energetic position and corresponding (artificial) k-value of the top of the band-tails distribution, and $E_{0,\mathrm{c/v}}$ is the Urbach energy. At the interface between a highly-doped and intrinsic region, the ballistic BTT model [16] assumes a decaying quasi-extended band-tails DOS into the intrinsic region, see Fig. 3. This imitates a direct proportionality between the band-tails DOS and the local doping concentration profile, which is assumed to have a steep gradient of 5 to $10\,\mathrm{nm/dec}$ at the interface. When calculating the BTT current contribution, I_{BTT}, it is assumed that only the quasi-extended band-tails (BT) states within a limited energy range ΔE_{edge} from the conventional band

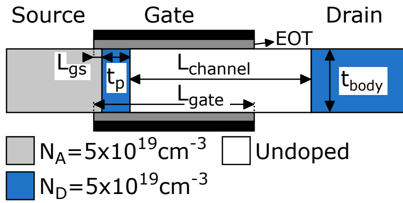

Fig. 1. Schematic structure of the pocketed homostructure *p-n-i-n* $In_{0.53}Ga_{0.47}As$ TFET with $\boldsymbol{L_{\text{channel}}}$=60 nm, $\boldsymbol{t_{\text{p}}}$=3 nm, $\boldsymbol{L_{\text{gs}}}$=1 nm, $\boldsymbol{t_{\text{body}}}$=10 nm, $\boldsymbol{L_{\text{gate}}}$=54 nm and $\mathbf{EOT}$=0.6 nm.

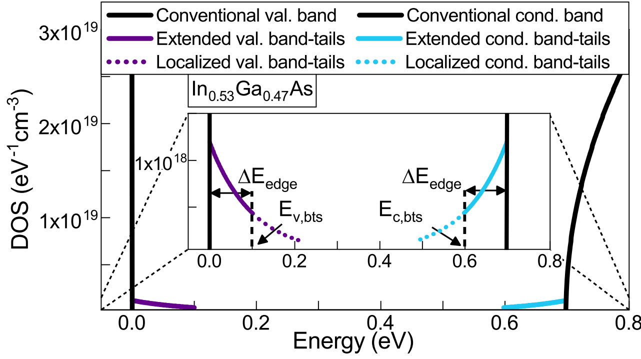

Fig. 2. The $In_{0.53}Ga_{0.47}As$ density-of-states (DOS) of the conventional valence and conduction band (black) together with the calibrated valence band-tails DOS (purple) and conduction band-tails DOS (blue) based on Eq. (1) of our band-tails model ($\boldsymbol{T}$=300 K). During calibration, the quasi-extended band-tails states (solid purple and blue) are assumed to extend into the bandgap over an energy range of $\boldsymbol{\Delta E_{\text{edge}}}$=100 meV. The abrupt transition from quasi-extended to localized band-tails states (dotted purple and blue) is indicated by $\boldsymbol{E_{\text{v,bts}}}$ and $\boldsymbol{E_{\text{c,bts}}}$. The axis labels of the main figure also apply to the inset.

edges, up to an energy $E_{\text{v,bts}}$ or $E_{\text{c,bts}}$ (see Fig. 2), contribute to the BTT current. In this work, the conventional band states are taken to be the electronic states of the ideal undoped material system. The ballistic BTT current itself consists of three tunneling contributions (Fig. 3): a) tunneling between quasi-extended valence and conduction BT states, $I_{\text{bts}\leftrightarrow\text{bts}}$, b) tunneling between conventional valence band states and conduction BT states, $I_{\text{v}\leftrightarrow\text{c,bts}}$, and c) tunneling between valence BT states and conventional conduction band states, $I_{\text{c}\leftrightarrow\text{v,bts}}$. The current density contributions are calculated using the Tsu-Esaki expression for ballistic tunneling [16]:

$$J_{\substack{\text{bts}\leftrightarrow\text{bts}\\ \text{v}\leftrightarrow\text{c,bts}\\ \text{c}\leftrightarrow\text{v,bts}}} = \frac{q}{2\pi^2\hbar}\int_{x_\text{l}}^{x_\text{r}} q\mathcal{E}(x)\int_{\forall k_\perp} k_\perp T(E_{\substack{\text{v,bts}\\ \text{v}\\ \text{v,bts}}}(x),k_\perp) \times \left[f_\text{n}(E_{\substack{\text{c,bts}\\ \text{c,bts}\\ \text{c}}}(x',k_\perp)) - f_\text{p}(E_{\substack{\text{v,bts}\\ \text{v}\\ \text{v,bts}}}(x,k_\perp))\right] \text{d}k_\perp \text{d}x \quad (2)$$

where $\mathcal{E}$ is the local electric field, $x_{\text{l/r}}$ is the left/right contact position, $k_\perp$ is the magnitude of the orthogonal wave vector, T is the transmission probability, $f_{\text{n/p}}$ is the electron/hole Fermi-Dirac distribution function, and $x' = x + l_{\text{tun}}$ with l_{tun} the tunnel-path length. Note that the calibration of both the models for BTBT and ballistic BTT is based on two highly-doped $In_{0.53}Ga_{0.47}As$ Esaki diodes at multiple temperatures [16]. The successful calibration of the entire *I-V* characteristics of these Esaki diodes suggests that it is justified to only consider high-doping-induced BTT and to neglect the temperature dependence of the BTT model parameters $E_{1,\text{c/v}}$, $k_{1,\text{c/v}}$, and

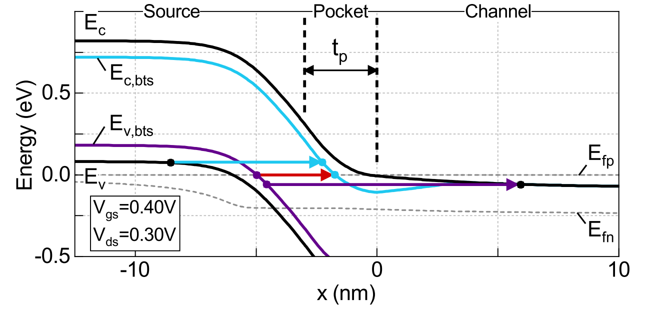

Fig. 3. Band diagram at the tunnel junction of the TFET of Fig. 1 for $\boldsymbol{V_{\text{gs}}}$ = 0.40 V ($\boldsymbol{T}$=300 K), showing the conventional valence and conduction band edges (black), the quasi-Fermi levels (dashed gray), the valence band-tails edge (purple), $\boldsymbol{E_{\text{v,bts}}}$, and the conduction band-tails edge (blue), $\boldsymbol{E_{\text{c,bts}}}$. The quasi-extended band-tails states have a limited penetration into the undoped channel. The different tunneling contributions to the BTT current (Eq. (2)) are indicated: a) $\boldsymbol{I_{\text{bts}\leftrightarrow\text{bts}}}$ (red arrow), b) $\boldsymbol{I_{\text{v}\leftrightarrow\text{c,bts}}}$ (blue arrow), and c) $\boldsymbol{I_{\text{v,bts}\leftrightarrow\text{c}}}$ (purple arrow).

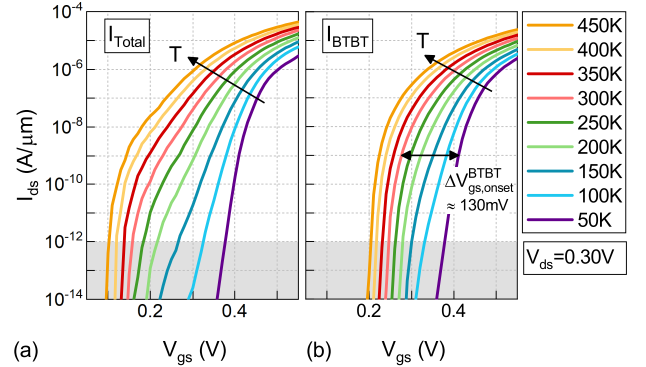

Fig. 4. Transfer characteristics of (a) $\boldsymbol{I_{\text{Total}}} = \boldsymbol{I_{\text{BTBT}}} + \boldsymbol{I_{\text{BTT}}}$ and (b) $\boldsymbol{I_{\text{BTBT}}}$ of the homostructure TFET of Fig. 1 as a function of temperature. For all simulations: $\boldsymbol{V_{\text{ds}}}$ = 0.30 V and $\boldsymbol{\Delta E_{\text{edge}}}$ = 100 meV. The shaded area indicates the irrelevant current levels.

$E_{0,\text{c/v}}$. The total current in the device of Fig. 1 is then found as: $I_{\text{Total}} = I_{\text{BTBT}} + I_{\text{BTT}}$. For the purpose of this work, currents induced by additional generation and recombination effects, such as Shockley-Read-Hall (SRH), are neglected.

III. Temperature Dependent Band-Tails Tunneling

A. Transfer characteristics

The transfer characteristics of the TFET are shown in Fig. 4 as a function of temperature for both I_{Total} and I_{BTBT}. In the case of I_{BTBT}, we can observe from Fig. 4(b) that the temperature dependence of the transfer characteristics is mainly reflected in an increase of the ON-current with temperature and a non-negligible shift of the onset voltage, $V_{\text{gs,onset}}^{\text{BTBT}}$, towards a lower V_{gs}. The onset voltage is defined as the gate-source ($V_{\text{gs,onset}}$) or drain-source ($V_{\text{ds,onset}}$) voltage for which $I_{\text{ds}} = 1\,\text{pA}/\mu\text{m}$. The temperature dependence of the conventional BTBT current I_{BTBT} has been demonstrated [19] to originate from an interplay between the temperature-dependent bandgap, described by the Varshni equation [20], and the temperature dependence of the Fermi-Dirac distribution and Fermi degeneracies. More specifically, there is an increase in tunneling efficiency because of the narrowing of the bandgap with temperature and there is a (limited) compensating effect because of a decreased internal electric field at the end of the tunneling path located in the channel [19]. This decrease of the

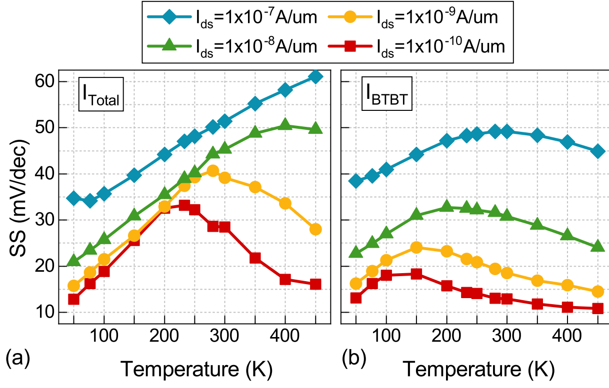

Fig. 5. Local subthreshold swing of (a) $\boldsymbol{I_{\mathrm{Total}} = I_{\mathrm{BTBT}} + I_{\mathrm{BTT}}}$ and (b) $\boldsymbol{I_{\mathrm{BTBT}}}$ of the TFET of Fig. 1 at specific current levels as a function of temperature, as extracted from the transfer characteristics in Fig. 4.

internal electric field with temperature can be traced back to the temperature dependence of the Fermi-Dirac distribution and Fermi degeneracies [19]. In III-V TFETs, the limited compensation of the tunneling efficiency results in a non-negligible temperature dependence of I_{BTBT}, as observed in Fig. 4(b)). This is in contrast to the often observed negligible temperature dependence in III-V Esaki diodes where a (nearly) full compensation occurs [19]. Note that the reported shift of $V_{\mathrm{gs,onset}}^{\mathrm{BTBT}}$ in Fig. 4(b) is consistent with the often observed strong temperature-dependent shift of $V_{\mathrm{gs,onset}}^{\mathrm{BTBT}}$ in measurements of BTBT-dominated TFETs ($90\,\mathrm{mV}$ shift at $1\,\mathrm{nA}/\mu\mathrm{m}$ between $300\,\mathrm{K}$ and $50\,\mathrm{K}$ in Ref. [21]).

The first signature of high-doping-induced ballistic BTT in the transfer characteristics is the increased temperature dependence of the SS, which can be observed from comparing the simulation results for I_{Total} (Fig. 4(a)) with those for I_{BTBT} (Fig. 4(b)). The SS, evaluated at multiple current levels, has been plotted in Fig. 5 as a function of temperature for both I_{Total} (Fig. 5(a)) and I_{BTBT} (Fig. 5(b)). The results reveal a linear dependence between the SS of I_{Total} and the temperature over a significant part of the considered temperature range. This is a clear indication that the BTT-based SS is thermally-limited, similarly to the SS of a MOSFET or TAT in a TFET. This is explained by the temperature dependence of the Fermi-Dirac distribution which has a significantly larger impact on the occupation probability of the states close to the band-tails edge, $E_{\mathrm{v/c,bts}}$ than on the conventional band states (Fig. 6). As an example, we can observe from Fig. 6 that the occupation probability, $\mathrm{f_{FD}}$, of a valence band-tails state at $E = E_{\mathrm{v,bts}}$ increases with a factor of about 10^{16} when the temperature is increased from $\mathrm{T} = 50\,\mathrm{K}$ to $\mathrm{T} = 450\,\mathrm{K}$. In comparison, for an identical increase of the temperature, the occupation probability of a conventional valence band state at $E = E_{\mathrm{v}}$ only increases with a factor of about 10^{7}. This is significant as the states close to the band-tails edge are the first to contribute to the BTT current, whereas the the states close to the conventional band edges are the first to contribute to the conventional BTBT current. As a result, the current, which depends on the occupation probability (Eq (2)), will increase more strongly with temperature for BTT than for BTBT.

After the initial linear increase with temperature, the SS of I_{Total}, especially at lower current levels, is seen to decrease

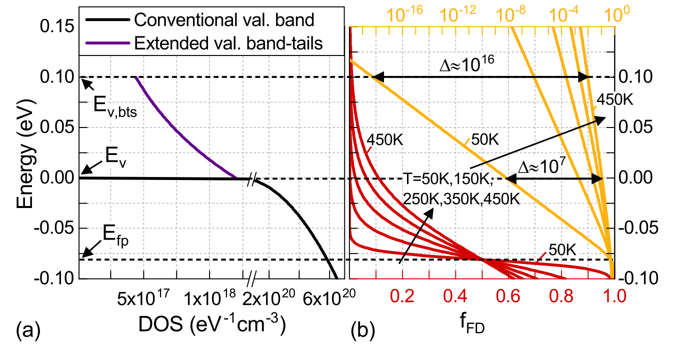

Fig. 6. (a) The $\mathrm{In_{0.53}Ga_{0.47}As}$ conventional valence band DOS (black) and valence band-tails DOS (purple) as a function of energy, with $\boldsymbol{\Delta E_{\mathrm{edge}}} = 100\,\mathrm{meV}$. The hole quasi-Fermi level, $\boldsymbol{E_{\mathrm{fp}}}$, conventional valence band edge, $\boldsymbol{E_{\mathrm{v}}}$, and the valence band-tails edge, $\boldsymbol{E_{\mathrm{v,bts}}}$, in the source (representative for $\mathbf{x} \leqslant -10\,\mathrm{nm}$ in Fig. 3) are indicated using dashed lines. (b) Fermi-Dirac occupation probability, $\mathbf{f_{FD}}$, as a function of the energy and temperature on both a linear (red lines, bottom x-axis) and a logarithmic (yellow lines, top x-axis) scale (note: the linear and logarithmic scale share the same vertical energy axis). The double-headed arrows indicate the difference in occupation probability between $\mathbf{T} = 450\,\mathrm{K}$ and $\mathbf{T} = 50\,\mathrm{K}$ at $\boldsymbol{E} = \boldsymbol{E_{\mathrm{v}}}$ and $\boldsymbol{E} = \boldsymbol{E_{\mathrm{v,bts}}}$, respectively.

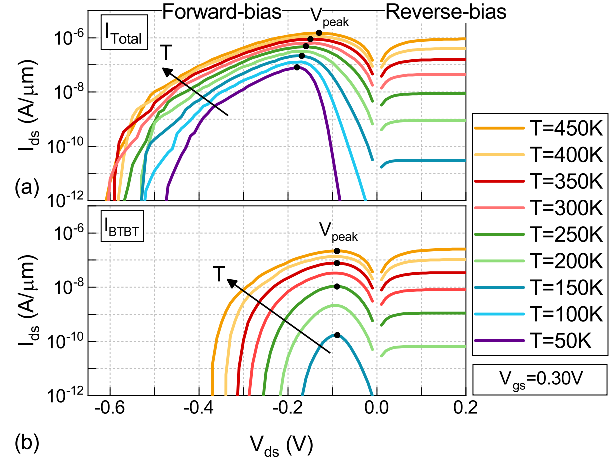

Fig. 7. Output characteristics of (a) $\boldsymbol{I_{\mathrm{Total}} = I_{\mathrm{BTBT}} + I_{\mathrm{BTT}}}$ and (b) $\boldsymbol{I_{\mathrm{BTBT}}}$ of the TFET of Fig. 1 as a function of temperature. The voltage corresponding to the peak of the forward-bias current, $\boldsymbol{V_{\mathrm{peak}}}$, is indicated (for clarity, the peak voltage is not shown for every curve). For all simulations: $\boldsymbol{V_{\mathrm{gs}}} = 0.30\,\mathrm{V}$ and $\boldsymbol{\Delta E_{\mathrm{edge}}} = 100\,\mathrm{meV}$.

with temperature (Fig. 4(a)). This reflects the abrupt onset of the ballistic BTT transitions which becomes observable at the onset voltage for I_{Total}, $V_{\mathrm{gs,onset}}^{\mathrm{Total}}$. In reality, the transition between quasi-extended and localized band-tails states is more gradual than what is assumed in our band-tails model and, therefore, the decrease of SS with increasing temperature at the lower current levels is expected to be less pronounced.

In summary, we have shown that a temperature-dependent SS in TFET, and in particular a linear increase of SS with temperature up to $300\,\mathrm{K}$, is also a signature of ballistic BTT and not only of a thermally-assisted process, such as TAT. This finding is in agreement with the experimental temperature dependence of SS as reported in Fig. 2(d) of Ref. [14].

B. Output characteristics

The output characteristics of the TFET are shown in Fig. 7 as a function of temperature for both I_{Total} and I_{BTBT}. For I_{BTBT}, the left-shift of $V_{\mathrm{ds,onset}}^{\mathrm{BTBT}}$ and increasing tunnel-

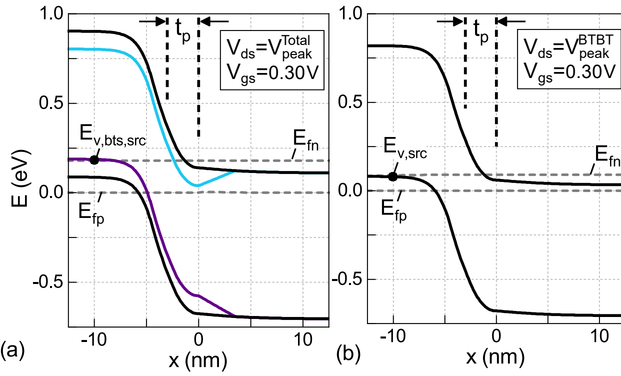

Fig. 8. Band diagram at the tunnel junction of the TFET of Fig. 1 for (a) $\boldsymbol{V_{\mathrm{ds}}=V_{\mathrm{peak}}^{\mathrm{Total}}}$ and (b) $\boldsymbol{V_{\mathrm{ds}}=V_{\mathrm{peak}}^{\mathrm{BTBT}}}$, showing the conventional band edges (black), quasi-Fermi levels (dashed gray) and the valence band-tails edge (purple) and conduction band-tails edge (blue). $\boldsymbol{T}$=300 K.

ing efficiency with temperature are again explained by the temperature-dependent bandgap and the temperature dependence of the Fermi-Dirac distribution and Fermi degeneracies.

In contrast to the first signature, the second signature of ballistic BTT is a decrease of the temperature dependence of I_{Total} in forward-bias ($V_{\mathrm{ds}} < 0\,\mathrm{V}$) in the output characteristics, compared to I_{BTBT}. The decrease in temperature dependence can be traced back to both the comparatively shorter tunneling paths and the more uniform electric field (similar to the electric field in an Esaki-diode) along the tunneling path compared to during a BTBT transition, at an identical V_{gs} (see Fig. 3). A shorter tunneling path results in a higher tunneling efficiency (approaching unity) and, consequently, the tunneling process becomes inherently less sensitive to variations (including temperature-induced variations). The more uniform electric field during BTT transitions also results in a more complete compensation of the bandgap narrowing-induced temperature dependence of the tunneling efficiency [19]. Note that, for similar reasons, the temperature dependence of I_{BTBT} is seen to decrease at larger V_{gs} (see Fig. 4 in Ref. [19]).

The third signature is the temperature dependence of the peak voltage, V_{peak}, defined as the voltage corresponding to the peak current in forward-bias (Fig. 7(a)). At low temperature, V_{peak} is set by the Fermi degeneracy in the source, $E_{\mathrm{fp,src}} - E_{\mathrm{v,src}}$, because, in the case of I_{BTBT}, V_{peak} is reached when the electron quasi-Fermi level in the channel, $E_{\mathrm{fn,ch}}$, which is set by V_{ds}, is approximately equal to the valence band edge energy in the source, $E_{\mathrm{v,src}}$ (Fig. 8(b)). Similarly, at low temperature and in the case of I_{Total}, V_{peak} is reached when $E_{\mathrm{fn,ch}} \approx E_{\mathrm{v,bts,src}} = E_{\mathrm{v,src}} + \Delta E_{\mathrm{edge}}$ (Fig. 8(a)).

For I_{BTBT}, V_{peak} only has a small temperature dependence, because temperature-dependent Fermi degeneracy changes in the source and Fermi-Dirac distribution changes in the channel seem to (mostly) compensate each other. In the case of I_{Total}, V_{peak} shifts to more positive V_{ds} as the relative contribution of I_{BTBT} to I_{Total} increases with temperature, shifting V_{peak} from $E_{\mathrm{fn,ch}} \approx E_{\mathrm{v,bts,src}}$ towards $E_{\mathrm{fn,ch}} \approx E_{\mathrm{v,src}}$. Our findings are in agreement with experimental data, as evident from Fig. 2 in Ref. [22], where the output characteristics show a small temperature-dependent shift of V_{peak} in the NDR regime for a V_{gs} with a BTBT-dominated current.

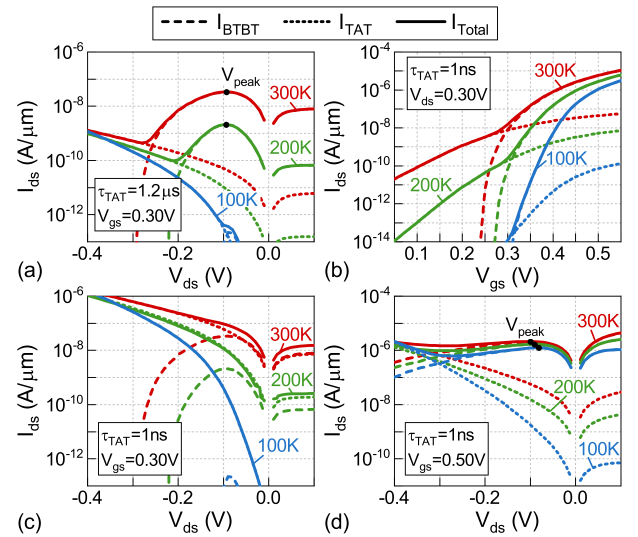

Fig. 9. (a) Output characteristics for $\boldsymbol{V_{\mathrm{gs}}} = 0.30\,\mathrm{V}$ of the TFET of Fig. 1 showing the conventional BTBT current, $\boldsymbol{I_{\mathrm{BTBT}}}$, the TAT current, $\boldsymbol{I_{\mathrm{TAT}}}$, and the total current, $\boldsymbol{I_{\mathrm{Total}} = I_{\mathrm{BTBT}} + I_{\mathrm{TAT}}}$ as a function of temperature. The TAT current simulations have been performed using the calibrated model parameters as described in Ref. [23] with a Huang-Rhys factor of $\mathbf{S} = \mathbf{13}$ and charge carrier lifetime of $\boldsymbol{\tau_{\mathrm{TAT}}} = 1.2\,\mu\mathrm{s}$, the original calibrated value in Ref. [23]. (b) Transfer characteristics for $\boldsymbol{V_{\mathrm{ds}}} = 0.30\,\mathrm{V}$ and $\boldsymbol{\tau_{\mathrm{TAT}}} = 1\,\mathrm{ns}$. (c)-(d) Output characteristics for $\boldsymbol{\tau_{\mathrm{TAT}}} = 1\,\mathrm{ns}$, and (c) $\boldsymbol{V_{\mathrm{gs}}} = 0.30\,\mathrm{V}$ and (d) $\boldsymbol{V_{\mathrm{gs}}} = 0.50\,\mathrm{V}$.

Lastly, note that, in contrast to the transfer characteristics, the signature of BTT in the output characteristics is predicted to be different from the signature of TAT. In the case of TAT, the current contribution increases with forward-bias, as shown in Fig. 9(a). The TAT current simulations in Fig. 9 have been performed using the dynamic non-local TAT model of Schenk [17], which has been calibrated against the experimental data of two $\mathrm{In_{0.53}Ga_{0.47}As}$ Esaki diodes (with similar doping profiles as the Esaki diodes used to calibrate our band-tails model [16]) at multiple temperatures in Ref. [23].

When using the calibrated parameter values [23], the forward-bias current is not dominated by TAT (Fig. 9(a)). Consequently, TAT has no impact on V_{peak} as it remains determined by $E_{\mathrm{fn,ch}} \approx E_{\mathrm{v,src}}$ and, therefore, only has a small temperature dependence. Assuming a negligible SRH contribution, the difference in signature between BTT and TAT in the output characteristics for a given V_{gs} can be used to distinguish between a TFET device of which the current is dominated by BTT or TAT at that given V_{gs}. More specifically, for a BTT-dominated TFET with degenerately doped source, drain and, if present, pocket regions, the output characteristics are expected to exhibit a well defined negative differential resistance (NDR) regime and a well identifiable V_{peak}, regardless of V_{gs} (see in Fig. 7(a)). In contrast, for a TAT-dominated TFET, the output characteristics are not expected to exhibit a well-defined NDR regime for those V_{gs} where the TAT current dominates the total current, as the TAT current increases with forward-bias (Fig 9(c) and (d)).

In Fig 9(c) and (d), we have artificially increased the TAT current contribution by decreasing the charge carrier lifetime, which is related to the amount of traps present in the system, from the calibrated $\tau_{\mathrm{TAT}} = 1.2\,\mu\mathrm{s}$ to $1\,\mathrm{ns}$. By setting $\tau_{\mathrm{TAT}} = 1\,\mathrm{ns}$, we ensure that the impact of TAT on

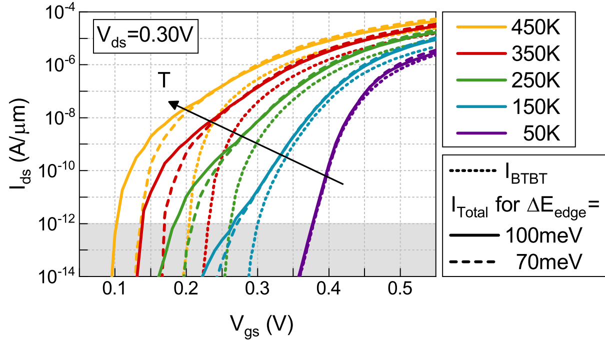

Fig. 10. Transfer characteristics ($V_{ds} = 0.30$ V) of I_{Total} and I_{BTBT} of the *p-n-i-n* TFET as function of temperature for different values of ΔE_{edge}.

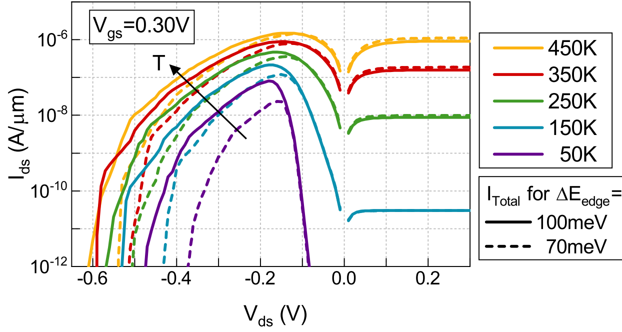

Fig. 11. Output characteristics ($V_{gs} = 0.30$ V) of I_{Total} of the *p-n-i-n* TFET as function of temperature for different values of ΔE_{edge}. For clarity, the corresponding I_{BTBT} output characteristics are not shown.

the transfer characteristics (Fig. 9(b)) becomes comparable to that of BTT (Fig. 4(a)). This results in a more relevant comparison between the output characteristics of the BTT-dominated TFET (Fig. 7(a)) and the TAT-dominated TFET (Fig 9(c) and (d)). From Fig 9(c), it is clear that the concept of V_{peak} becomes meaningless when the forward-bias current is dominated by TAT, as the NDR regime is suppressed entirely by the TAT current. Only when the device current is dominated by conventional BTBT (at large V_{gs}), an NDR regime exists in the output characteristics (Fig 9(d)).

C. Energetic extension of band-tails states

This section explores how varying ΔE_{edge} affects the simulated transfer (Fig. 10) and output (Fig. 11) characteristics. ΔE_{edge} is the assumed energy range, starting from the conventional band edges, within which band-tails states are considered to be quasi-extended states. During all simulations, the appropriate set of calibrated parameters for the band-tails model have been used [16].

From both Fig. 10 and Fig. 11, it can be seen that ΔE_{edge} mainly affects the transfer and output characteristics around the ΔE_{edge}-dependent onset voltage for tunneling, $V_{gs,onset}^{Total}$ and $V_{ds,onset^{Total}}$. As expected, a larger ΔE_{edge} results in a shift of $V_{gs,onset}^{Total}$ towards more negative V_{gs} and of $V_{ds,onset^{Total}}$ towards more negative V_{ds}. In the case of the transfer characteristics, the onset of BTT is achieved when the gate-source voltage has aligned the conduction band-tails state at $E_{c,bts,ch}$ with the valence band-tails state at $E_{v,bts,src}$, as illustrated in Fig. 12(a). $E_{c,bts,ch}$ is defined as the conduction band-tails state with the lowest energy (at that

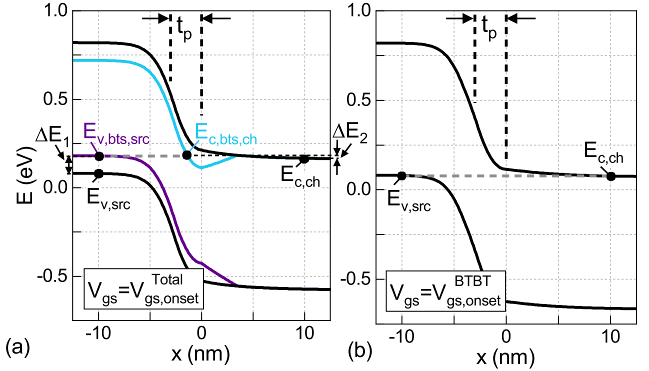

Fig. 12. Band diagram at the tunnel junction of the TFET of Fig. 1 for (a) $V_{gs}=V_{gs,onset}^{Total}$ and (b) $V_{gs}=V_{gs,onset}^{BTBT}$, showing the conventional band edges (black) and the valence band-tails edge (purple) and conduction band-tails edge (blue). T=300 K. The gray dashed line indicates the first energy level for which ballistic tunneling between (a) the valence band-tails states in the source and the conduction band-tails states in the channel or (b) the conventional valence band states in the source and the conventional conduction band states in the channel becomes available. (a)-(b) $V_{ds} = 0.3$ V.

V_{gs}) for which a ballistic path exists that does not penetrate any electrostatic potential barriers between that state and the drain contact (hence limited attenuation). Similarly, $E_{v,bts,src}$ is defined as the valence band-tails state in the source with the highest energy for which also a ballistic path exists that does not penetrate any electrostatic potential barriers between that state and the source contact. Note that the conduction band-tails state at $E_{c,bts,ch}$ does not necessarily correspond to the conduction band-tails state with the overall lowest energy in the channel because we require there to be a ballistic path (and no electrostatic potential barriers except for the forbidden gap transition) from source contact to drain contact (Fig. 12(a)).

The onset of conventional BTBT, is achieved when the gate-source voltage has aligned the conventional conduction band edge in the channel at $E_{c,ch}$ with the conventional valence band edge in the source at $E_{v,src}$ (Fig. 12(b)), where $E_{c,ch}$ and $E_{v,src}$ are the energy levels of the conventional band edges in the neutral channel and source, respectively. There is a shift in gate-source onset voltage, $\Delta V_{gs,onset}^{BTT\text{-}BTBT} = V_{gs,onset}^{BTBT} - V_{gs,onset}^{Total}$, since at $V_{gs} = V_{gs,onset}^{Total}$, $E_{c,ch}(V_{gs,onset}^{Total}) = E_{v,src} + \Delta E_1 - \Delta E_2$, with $\Delta E_1 = E_{v,bts,src} - E_{v,src}$ and $\Delta E_2 = E_{c,bts,ch}(V_{gs,onset}^{Total}) - E_{c,ch}(V_{gs,onset}^{Total})$ (Fig. 12(a)):

$$\begin{aligned}\Delta V_{gs,onset}^{BTT\text{-}BTBT} &= \int_{E_{c,ch}(V_{gs,onset}^{Total})}^{E_{c,ch}(V_{gs,onset}^{BTBT})} \frac{1}{\mathrm{d}E_{c,ch}(V_{gs})/\mathrm{d}V_{gs}} \mathrm{d}E_{c,ch} \\ &= \frac{-1}{\mathrm{d}E_{c,ch}(V_{gs'})/\mathrm{d}V_{gs}} \left[\Delta E_1 - \Delta E_2\right], \end{aligned} \tag{3}$$

where we have used the 'Mean Value Theorem' with $V' \in \left[V_{gs,onset}^{Total}, V_{gs,onset}^{BTBT}\right]$. Since $\mathrm{d}E_{c,ch}(V'_{gs})/\mathrm{d}\left(qV_{gs}\right) \approx -1$, $\Delta E_1 = \Delta E_{edge}$, and $\Delta E_2 \approx 0$, Eq. (3) reduces to:

$$\Delta V_{gs,onset}^{BTT\text{-}BTBT} \approx \left(\Delta E_1 - \Delta E_2\right)/q \approx \Delta E_{edge}/q \tag{4}$$

As a result, $\Delta V_{gs,onset}^{BTT\text{-}BTBT}$ provides information on ΔE_{edge}. In practice, only $V_{gs,onset}^{Total}$ is experimentally accessible and careful simulation efforts are therefore required to extract ΔE_{edge} from experimental data. Note that a sufficiently high temperature is assumed such that I_{Total} is BTT-dominated around

$V_{\mathrm{gs,onset}}^{\mathrm{Total}}$ or $V_{\mathrm{ds,onset}}^{\mathrm{Total}}$. In addition, note that experimental data may suffer from a temperature-dependent contact resistance.

Lastly, in the case of the transfer characteristics, it is clear that ΔE_{edge} has a negligible impact on I_{on} and only affects the SS close to $V_{\mathrm{gs,onset}}^{\mathrm{Total}}$ despite the change in calibrated value of the band edge decay parameter E_0, which comes along with the change in ΔE_{edge}. This result is consistent with the earlier finding that the SS of I_{Total} is determined by the density of quasi-extended band-tails states in a small energy range in the bandgap and not by the band edge decay parameter E_0 (see Eq. (1)) [16]. Similarly, ΔE_{edge} has a negligible impact on the output characteristics in reverse-bias.

IV. Conclusion

In conclusion, ballistic BTT significantly increases the temperature dependence of the TFET's SS towards a linear dependence on temperature up to room temperature. Such a temperature dependence is observed in many experimental data. Our work therefore demonstrates that an SS proportional to temperature in TFET is not only a signature of TAT. To distinguish BTT from TAT, the output characteristics in forward-bias should be studied. The output characteristics of a BTT-dominated TFET are predicted to exhibit a NDR regime, regardless of V_{gs}. In contrast, the output characteristics of a TAT-dominated TFET are predicted to exhibit a NDR regime only at large V_{gs}, as the TAT current conceals the NDR regime at small V_{gs}. Lastly, an approximate expression relating the shift of the gate-source onset voltage with the energetic extension, ΔE_{edge}, of band-tails states in the bandgap has been proposed and can be used to extract ΔE_{edge} from comparing temperature-dependent experiments to simulations.

Acknowledgment

The authors would like to thank Quentin Smets for his helpful assistance with the TAT simulations and Andreas Schenk for insightful discussions about band-tails.

References

[1] A. M. Ionescu and H. Riel, "Tunnel field-effect transistors as energy-efficient electronic switches," *Nature*, vol. 479, no. 7373, pp. 329–337, nov 2011, doi: http://doi.org/10.1038/nature10679.

[2] H. Lu and A. Seabaugh, "Tunnel Field-Effect Transistors: State-of-the-Art," *IEEE Journal of the Electron Devices Society*, vol. 2, no. 4, pp. 44–49, jul 2014, doi: http://doi.org/10.1109/JEDS.2014.2326622.

[3] D. Verreck, G. Groeseneken, and A. S. Verhulst, "The Tunnel Field-Effect Transistor," in *Wiley Encyclopedia of Electrical and Electronics Engineering*. Hoboken, NJ, USA: John Wiley & Sons, Inc., 2016, pp. 1–24, doi: http://doi.org/10.1002/047134608X.W8333.

[4] U. E. Avci, D. H. Morris, and I. A. Young, "Tunnel Field-Effect Transistors: Prospects and Challenges," *IEEE Journal of the Electron Devices Society*, vol. 3, no. 3, pp. 88–95, may 2015, doi: http://doi.org/10.1109/JEDS.2015.2390591.

[5] A. Krishnaraja, J. Svensson, E. Lind, and L. E. Wernersson, "Reducing ambipolar off-state leakage currents in III-V vertical nanowire tunnel FETs using gate-drain underlap," *Applied Physics Letters*, vol. 115, no. 14, p. 143505, 2019, doi: http://doi.org/10.1063/1.5115296.

[6] J. Charles, P. Sarangapani, R. Golizadeh-Mojarad, R. Andrawis, D. Lemus, X. Guo, D. Mejia, J. E. Fonseca, M. Povolotskyi, T. Kubis, and G. Klimeck, "Incoherent transport in NEMO5: realistic and efficient scattering on phonons," *Journal of Computational Electronics*, vol. 15, no. 4, pp. 1123–1129, dec 2016, doi: http://doi.org/10.1007/s10825-016-0845-y.

[7] S. Sant, K. Moselund, D. Cutaia, H. Schmid, M. Borg, H. Riel, and A. Schenk, "Lateral InAs/Si p-Type Tunnel FETs Integrated on Si—Part 2: Simulation Study of the Impact of Interface Traps," *IEEE Transactions on Electron Devices*, vol. 63, no. 11, pp. 4240–4247, nov 2016, doi: http://doi.org/10.1109/TED.2016.2612484.

[8] M. Mohammed, A. S. Verhulst, D. Verreck, M. Van de Put, E. Simoen, B. Sorée, B. Kaczer, R. Degraeve, A. Mocuta, N. Collaert, A. Thean, and G. Groeseneken, "Electric-field induced quantum broadening of the characteristic energy level of traps in semiconductors and oxides," *Journal of Applied Physics*, vol. 120, no. 24, p. 245704, 2016, doi: http://doi.org/10.1063/1.4972482.

[9] J. T. Teherani, S. Agarwal, W. Chern, P. M. Solomon, E. Yablonovitch, and D. A. Antoniadis, "Auger generation as an intrinsic limit to tunneling field-effect transistor performance," *Journal of Applied Physics*, vol. 120, no. 8, 2016, doi: http://doi.org/10.1063/1.4960571.

[10] S. Sant and A. Schenk, "The effect of density-of-state tails on band-to-band tunneling: Theory and application to tunnel field effect transistors," *Journal of Applied Physics*, vol. 122, no. 13, p. 135702, 2017, doi: http://doi.org/10.1063/1.4994112.

[11] M. A. Khayer and R. K. Lake, "Effects of band-tails on the subthreshold characteristics of nanowire band-to-band tunneling transistors," *Journal of Applied Physics*, vol. 110, no. 7, p. 074508, 2011, doi: http://doi.org/10.1063/1.3642954.

[12] H. Zhang, W. Cao, J. Kang, and K. Banerjee, "Effect of band-tails on the subthreshold performance of 2D tunnel-FETs," in *2016 IEEE International Electron Devices Meeting (IEDM)*. IEEE, dec 2016, pp. 30.3.1–30.3.4, doi: http://doi.org/10.1109/IEDM.2016.7838512.

[13] S. Agarwal and E. Yablonovitch, "Band-Edge Steepness Obtained From Esaki/Backward Diode Current-Voltage Characteristics," *IEEE Transactions on Electron Devices*, vol. 61, no. 5, pp. 1488–1493, may 2014, doi: http://doi.org/10.1109/TED.2014.2312731.

[14] E. Memisevic, E. Lind, M. Hellenbrand, J. Svensson, and L.-E. Wernersson, "Impact of Band-Tails on the Subthreshold Swing of III-V Tunnel Field-Effect Transistor," *IEEE Electron Device Letters*, vol. 38, no. 12, pp. 1661–1664, dec 2017, doi: http://doi.org/10.1109/LED.2017.2764873.

[15] S. Sant, Q. Ding, M. Rau, M. Luisier, and A. Schenk, "Variability in the Characteristics of InGaAsSb/InAs Tunnel FETs Caused by Dopant-induced Traps," in *2019 Electron Devices Technology and Manufacturing Conference (EDTM)*. IEEE, mar 2019, pp. 112–114, doi: http://doi.org/10.1109/EDTM.2019.8731238.

[16] J. Bizindavyi, A. S. Verhulst, Q. Smets, D. Verreck, B. Soree, and G. Groeseneken, "Band-Tails Tunneling Resolving the Theory-Experiment Discrepancy in Esaki Diodes," *IEEE Journal of the Electron Devices Society*, vol. 6, no. June, pp. 633–641, 2018, doi: http://doi.org/10.1109/JEDS.2018.2834825.

[17] *Sentaurus Device User Guide, Version N-2017.09*, Synopsys, Mountain View, CA, USA, 2018.

[18] J. Bizindavyi, A. S. Verhulst, B. Soree, and G. Groeseneken, "Impact of calibrated band-tails on the subthreshold swing of pocketed TFETs," in *2018 76th Device Research Conference (DRC)*, vol. 2018-June, no. 2017. IEEE, jun 2018, pp. 1–2, doi: http://doi.org/10.1109/DRC.2018.8442246.

[19] J. Bizindavyi, A. S. Verhulst, D. Verreck, B. Soree, and G. Groeseneken, "Large Variation in Temperature Dependence of Band-to-Band Tunneling Current in Tunnel Devices," *IEEE Electron Device Letters*, vol. 40, no. 11, pp. 1864–1867, nov 2019, doi: http://doi.org/10.1109/LED.2019.2939668.

[20] Y. Varshni, "Temperature dependence of the energy gap in semiconductors," *Physica*, vol. 34, no. 1, pp. 149–154, jan 1967, doi: http://doi.org/10.1016/0031-8914(67)90062-6.

[21] A. Alian, Y. Mols, C. C. Bordallo, D. Verreck, A. Verhulst, A. Vandooren, R. Rooyackers, P. G. Agopian, J. A. Martino, A. Thean, D. Lin, D. Mocuta, and N. Collaert, "InGaAs tunnel FET with sub-nanometer EOT and sub-60 mV/dec sub-threshold swing at room temperature," *Applied Physics Letters*, vol. 109, no. 24, 2016, doi: http://doi.org/10.1063/1.4971830.

[22] S. Mookerjea, D. Mohata, T. Mayer, V. Narayanan, and S. Datta, "Temperature-Dependent I–V Characteristics of a Vertical $In_{0.53}Ga_{0.47}As$ Tunnel FET," *IEEE Electron Device Letters*, vol. 31, no. 6, pp. 564–566, jun 2010, doi: http://doi.org/10.1109/LED.2010.2045631.

[23] Q. Smets, A. S. Verhulst, E. Simoen, D. Gundlach, C. Richter, N. Collaert, and M. M. Heyns, "Calibration of Bulk Trap-Assisted Tunneling and Shockley-Read-Hall Currents and Impact on InGaAs Tunnel-FETs," *IEEE Transactions on Electron Devices*, vol. 64, no. 9, pp. 3622–3626, 2017, doi: http://doi.org/10.1109/TED.2017.2724144.